Magnetic Resonance imaging (MRI) in detection of *Bifidobacterium longum* and *Clostridium novyi-NT* labeled with superparamagnetic iron oxide (SPIO) nanoparticle

Introduction

Nonpathogenic anaerobes can anchor and proliferate within solid tumors' hypoxia area. These microorganisms have been used for cancer diagnosis and therapy[1-6]. In order to develop effective anaerobic anticancer therapies, the location, distribution and long-term viability of these bacteria must be evaluated in a noninvasive manner. MRI of bacteria labeled with superparamagnetic iron oxide (SPIO) nanoparticles after either direct local injection or intravenous infusion might has the potential to fulfill this goal.

To determine the spatial and temporal progression of infections in live animals with implanted tumors, the tumor-specific amplification process was visualized in real time using luciferase-catalyzed luminescence and green fluorescent protein fluorescence, which revealed the locations of the tumors and metastases[7]. Magnetic resonance imaging (MRI) has the ability and been used widely to provide extremely sensitive, high-resolution images of magnetically labeled cells (such as stem cells) compared with optical and positron emission tomography scanning techniques. Similarly, we propose that it could also provide high-resolution imaging when it was performed to image magnetically labeled anaerobes. As such, the application of MRI to anaerobes investigations is of great importance to enhancing the development of bacteria oncolysis therapies.

However, to our knowledge, there are no researches about anaerobes tagging with SPIO nanoparticles and no coherent evaluations using MRI in vitro and in vivo. In present study, SPIO nanoparticles are utilized novelly to magnetically label *Bifidobacterium longum* (B.*longum*) and *Clostridium novyi-NT* (C.*novyi*-NT), and these microorganisms have been exploited in anerobes oncolysis for many years.

This is a first step towards anaerobes detection with noninvasive, continuous MRI that holds promise as an assessment tool for bacteriolytic anti-cancer therapies.

Materials and Methods

Bacterial Strains

The B.*longum* tested in this study was purchased from Shanghai Nature Biotechnology. The C.*novyi*-NT spore was provided by professors Bert Vogelstein & Kenneth W. Kinzler (Johns Hopkins University, USA).

Superparamagnetic Iron Oxides

Ferucarbotran (SHU 555 A, Resovist®, Schering AG, Berlin, Germany) is a clinically established contrast agent for magnetic resonance imaging. It consists of SPIO nanoparticles (average diameter, 65 nm, and core size, 3-5 nm) coated with carboxydextran. One millilitre solution contains 540 mg Ferucarbotran, corresponding to 0.5 mmol (28mg) iron. SPIO-based contrast agents mainly act on R_2 ($1/T_2$) and R_2^* ($1/T_2^*$) relaxation rates.

Cultural Medium and Condition

PYG liquid medium (PYG BrothBase, EHSY lab) contains: soy peptone 0.5g, tryptone (oxoid) 0.5g, yeast powder (oxoid) 1.0g, glucose 1.0g, inorganic salt solution 4 ml, distilled water 100ml, CYS muriat 0.05g, agar 1.5-2.0% medium, chlorhaematin and vitamin K1 were added when culture begin. The B.*longum* was cultured anaerobically at 37℃, PH 7.0 in the PYG medium.

The liquid or solid Reinforced Clostridial Medium (RCM) was employed to culture C.*novyi*-NT.

B.*longum* and C.*novyi*-NT tagging with SPIOs

All the procedures were performed under anerobic condition. The cultures were divided into four groups (six tubes in each group): (1) G (B.*longum*-SPIO): B.*longum* was inoculated anerobically in 50 ml PYG liquid medium, then 50 μl Ferucarbotran were employed as tagging reagents (28 μg/mL iron in incubation medium). (2) G (Free-SPIO): 50 ml PYG liquid medium doped only with 50 μl Ferucarbotran (28 μg/mL iron in incubation medium); (3) G (B.*longum*): only B.*longum* was inoculated anerobically in 50 ml PYG liquid medium and no Ferucarbotran. (4) G (Medium): neither bacteria nor SPIOs was added in the PYG medium. All the tubes were shaking cultured at 37□ for 72h.

The same methods were employed to label C.*novyi*-NT. The cultures were also divided into four groups: G (C.*novyi*-NT-SPIO); G (Free-SPIO); G (C.*novyi*-NT) and G (Medium).

Bacteria activity

Bacteria viability was determined with plate count test. In this assay, bacteria viability is determined by the colony number. Only live bacterium can form bacteria colony whereas dead bacterium can't. The B.*longum*-SPIO and B.*longum* were spread on culture plate with microamount inoculating loop (1μl) after series dilution, cultured under anaerobic condition for 72 hr, and finally bacteria number was calculated and recorded.

Electron microscopy

We examined the presence and morphology of SPIO particles using transmission electron microscopy after three days shaking culture. The samples of B.*longum*-SPIO, B.*longum*, C.*novyi*-NT-SPIO and C.*novyi*-NT were put into four eppendorf tubes with 1 mL per tube for centrifuge (10000 rpm/min) respectively. All the samples were fixed with stationary liquid (1% dilution of 6% tannin acid and 25% glutaraldehyde). Finally, transmission electron microscopy (CM120 electron microscopy, philips, Holland) was performed. Analyses were performed by using magnifications ranging from x10000 to x40000.

Animals

All animal studies were conducted according to a protocol approved by the Institute Animal Care Committee at The University of Fudan, Shanghai, China. Inbred Strain Buffalo rats weighting 200-250 g, which were provided by Animal Center of Medical College of Fudan University (original source, Charles River Laboratories, Wilmington, Mass), were used in this study. The animals were kept under conventional conditions (temperature 22 ± 2□, relative humidity 55 ± 10%, dark-light rhythm 12 hr) and had free access to laboratory chow and tap water.

Cell lines and culture

The rat hepatocellular carcinoma (HCC) cell line McA-RH7777 commercially available from American Type Culture Collection (ATCC number*:* CRL-1601™), was routinely grown in *DMEM (*Dulbecco's modified Eagle's medium*,* Mediatech*)*, supplemented with 4 mM L-glutamine adjusted to contain 1.5 g/L sodium bicarbonate and 4.5 g/L glucose, 90%; fetal bovine serum, 10%. The cells were incubated in 5% CO2 at 37℃. On the day of inoculation, cells were trypsinized and resuspended in DMEM medium at a final concentration of 2×10^6 cells per milliliter.

Innoculation

Subcutaneous tumors

All surgical and imaging procedures were performed under the condition of anesthesia. Six Buffalo rats weighting 200-250 g were anesthetized with ketamine hydrochloride (50 mg/kg body weight) after preanesthesia with diazepam (10 mg/kg body weight). Tumors were inoculated bilaterally on the back, approximately 1 cm distal to the scapula and 1 cm lateral to the midline, by means of subcutaneous injection of 250 μL of the cell suspension (5×10^5 cells), respectively.

Orthotopic hepatic tumors

About 5×10^5 McA-RH7777 cancer cells in 250 μL of DMEM—were injected into the flank of one Buffalo rat. When the tumor grew to approximately 10 mm in diameter, the animal was killed humanely, and the tumor was harvested for implantation into the rat livers. Twelve Buffalo rats were implanted with tumors in hepatic lobe. After intraperitoneal administration of ketamine (50 mg/kg) for anesthesia, laparotomy was performed through a midline abdominal incision, the hepatic lobe was exposed, and a small cut on the liver surface was made with a sharp scalpel. Fresh tumor tissue measuring 1×1×1 mm was embedded in the liver parenchyma of each rat. The cut was then kept on pressure to stop bleeding for 5 minutes with a cotton-tipped applicator, and the abdomen was sutured. Tumor inoculations were performed by one of the authors.

MRI of bacterial Phantoms

Four phantom groups, each group consisted of six phantoms, filled with medium that contained SPIO-labeled bacteria, Free-SPIO (non–bacteria-bound), bacteria and none, respectively, were prepared for MR imaging to qualitatively and quantitatively detect the differences between them.

Each phantom consisted of six tubes filled with medium that contained different concentrations of free (non–bacteria-bound) SPIO or SPIO-labeled bacteria. Two phantom setups were prepared for MRI: *(a)* To determine the effect of different SPIO concentration, a series of decreasing SPIO concentration (28, 14, 7, 3.5, and 1.75 μg of iron per milliliter of medium; three samples each) in the medium. *(b)* Different numbers (0.25×10^6, 0.5×10^6, 1×10^6, 2×10^6 and 4×10^6 B.*longum*-SPIO per milliliter of medium, three samples each) of iron-loaded bacteria were prepared; The number of SPIO-loaded bacteria was determined by bacteria plate culture under anaerobic condition.

The bacteria phantoms imaging was performed with a 3.0-T clinical whole-body MR unit (Signa EXITE 3.0T MRI, GE Healthcare) by using a 8 channel high resolution brain coil (HRBRAIN). T_2^* maps were obtained by using a Multi-gradient-echo sequence. For each gradient echo, full k-space was sampled and a series of images was reconstructed at different echo times. To avoid phase effects from eddy currents, the even and odd echoes were treated separately. For the phantom experiments, 6 gradient echoes were used to reconstruct a time series of images for T_2^* determination (160-msec repetition time, 2.4-msec interval between two uneven echoes, 30° flip angle, 256 × 256 spatial resolution, 2-mm section

thickness, 210-mm field of view. T_2 maps were acquired by using a Fast Spin Echo (FSE) multi-echo sequence (8 echoes, 500-msec TR, 7.9-msec interval between two echoes, 128×128 spatial resolution, 4-mm section thickness, 210-mm field of view, 90° flip angle). To suppress susceptibility influences in the gradient-echo sequence, measurements were performed with a high spatial resolution (256×256) and a low section thickness (2 mm). Because the spin-echo sequence is not strongly influenced by susceptibility artifacts, a lower spatial resolution (128×128) and a higher section thickness 4mm could be used to optimize the signal-to-noise ratio. These parameters did not influence the relaxation time results owing to the homogeneous in vitro models.

The R_2^* maps and R_2 maps were obtained by postprocessing with the Functool 4.5.3 software on the workstation (AWD, version 4.3, Research System, GE Healthcare). The R_2 and R_2^* were determined by using a Levenberg-Marquardt algorithm for every voxel. The mean relaxation rate per tube was determined by calculating the mean R_2^* and R_2 values within the diameter of the tube, which contained about 100 voxels. The homogeneous distribution of the bacteria in the medium was qualitatively and quantitatively tested by means of visual inspection of the R_2 and R_2^* maps to ensure that there were no hot spots of accumulated iron-labeled bacteria.

MR Imaging of in Vivo Experiments

To assess the performance of relaxometry in vivo, the culture solutions were subcutaneously bilaterally injected into the twelve subcutaneous tumors of six Buffalo rats (Charles River Laboratories, USA). The total volume of solution injected (1 mL) contained *(a)* B.*longum*-SPIO per milliliter of medium (4×10^6 cfu/ml) labeled with 28 μg/mL iron (n=6 tumors), *(b)* Free-SPIO per milliliter of medium (28 μg/mL iron) (n=6 tumors).

For orthotopic hepatic tumor, Twelve Buffalo rats were anesthetized by means of intraperitoneal injection of ketamine (50 mg per kilogram of body weight) and diazepam (10 mg/kg). B.*longum*-SPIO per milliliter of medium (4×10^6 cfu/ml) (n=6) or Free-SPIO per milliliter of medium (28 μg/mL iron) (n=6) were injected via tail vein. MRI were performed before and 15 days after injection. These animals were sacrificed after 15 days, and histopathologic findings were correlated with findings on MR images.

All the animals were transferred to the MR unit (Signa EXITE, GE Healthcare) and

into a custom-made smallanimal solenoid coil (60 mm in diameter and 150 mm in length) (GE Research Laboratories), and the head-to-tail symmetry line was placed perpendicular to B0 in the magnet bore. Transverse high-spatial resolution T_2-weighted MR images of tumor were acquired for visualizing anatomic details by using a fast spin-echo sequence with the following parameters: 2000/80 (TR msec/echo time msec), a 3-mm section thickness, a 0.2-mm intersection gap, a 512×512 matrix, and a 60×60-mm field of view. For in vivo T_2^* relaxometry, 6 gradient echoes were acquired by using a Multi-gradient-echo sequence (477-msec TR, 2.4-msec interval between two echoes, 256 × 256 spatial resolution, 2-mm section thickness, 60-mm field of view, flip angle 30°). For in vivo T_2 relaxometry, the same location was measured with 8 spin echoes (500-msec TR, 7.9- msec interval between two echoes, 128×128 spatial resolution, 4-mm section thickness, 60-mm field of view, 90° flip angle). The R_2^* maps and R_2 maps were also obtained by postprocessing with the Functool 4.5.3 software on the workstation (AWD, version 4.3, Research System, GE Healthcare).

Detection of Iron with Light Microscope by Iron staining

For bacterial smear, the bacteria were air dried and fixed on the slide by heating for Prussian blue staining in accordance with Iron Staining kit (genmed, USA). Both iron-loaded and nonlabeled control bacteria were examined by using a microscope (Nikon 80i, Japan) with a magnification of ×1000.

For tissue specimens, sections were cut at a thickness of 4 μm. After deparaffinage, hydration and dry, Prussian blue staining was performed according to Iron Staining kit (genmed, USA). Then the slides were examined with a microscope at magnifications from ×40 to×1000. Digital images were acquired by using a Nikon DXM1200 camera (Nikon, Japan) and ACT1/DXM1200F software (Nikon, Japan).

Statistic analysis

All the measurement data were expressed as $\bar{x} \pm s$. The differences of bacterial number in the bacteria activity test was compared by *t* test for two independent samples. Variance analysis was employed to compare R_2^* values or R_2 values among difference groups. The One-Way ANOVA was used to compare the effect of different SPIO concentration and different distribution (bacteria-SPIO or Free-SPIO) on R_2^* or R_2 value. A P value <0.05 was considered to indicate a significant difference. Computer software packages (SPSS, version 15.0 for windows, SPSS Inc, Chicago, Ill).

Results

Bacteria culturing, SPIO labeling and bacteria activity

After shaking culture anerobically for 72 hr, Bacteria pellets could be viewed in the culture tube of G (B.*longum*-SPIO), G (B.*longum*), G (C.*novyi*-NT-SPIO) and G (C.*novyi*-NT) after centrifuge (5000 rpm/min) for 10 min, while no pellets could be seen in the culture tube of G (medium) and G (Free-SPIO). The B.*longum*-SPIO pellets showed rust, even and opaque, while the color of its medium becomes light when compared with that of Free-SPIO. The B.*longum* pellets showed ivory white, even and opaque, and the color of its medium was similar with that of B.*longum*-SPIO's medium. There was no any sediment in the culture tubes of G (Free-SPIO) and G (Medium) (Fig 1). After anaerobic culture, the bacterial colony count in G (B.*longum*-SPIO) and in G (B.*longum*) was $(4.07\pm1.97)\times10^6$ cfu/ml and $(3.97\pm1.86)\times10^6$ cfu/ml, respectively, and there was no significant statistics difference between the two groups (P=0.69). This result perhaps indicated that the B.*longum*'s activity wasn't influenced by culturing with SPIO together.

Electron microscopy

The characteristic granular morphology of these SPIO particles was identified only in SPIO-labeled bacteria (B.*longum*-SPIO and C.*novyi*-NT-SPIO) and never in unlabeled controls (B.*longum* and C.*novyi*-NT). The unique appearance of SPIO particles is quite distinct from the morphology of other bacteria elements. The B.*longum*-SPIO contains a characteristic electron-dense sphere, ellipse or irregular-shaped crystals (about 50-100 nm) which mainly deposited along the midline of or dispersed within the bacteria body (Fig 2-a, 2-b). Similar crystals were also observed in the plasm of C.*novyi*-NT-SPIO. Of particular interest was the observation that these crystals were also trapped to the C.*novyi*-NT spores (Fig 2-c, 2-d).

Prussian blue staining

Iron in the B.*longum*-SPIO and C.*novyi*-NT-SPIO resulted in blue staining (Fig 3-a, 3-c), whereas B.*longum* and C.*novyi*-NT showed no blue staining by Prussian Blue Staining (Fig 3-b, 3-d).

MRI of bacteria phantom

All phantoms' solvent was bacteria medium in our experiments. A homogeneous distribution of the bacteria within the phantom was confirmed at visual inspection of the MR images. The effects of B.*longum*-SPIO, Free-SPIO,

B.*longum* and PYG Medium on R_2^* and R_2 were nicely visualized on the phantom images (Fig 4a, 4b). C.*novyi*-NT-SPIO, Free-SPIO, C.*novyi*-NT and RCM Medium had similar imaging (data not show).

The R_2^* value of B.*longum*-SPIO (273.25 sec-1 ± 22.35) was significantly higher than that of Free-SPIO (125.63 sec^{-1} ± 2.19) (P<0.001), however, the R_2^* value of B.*longum* (5.83 sec^{-1} ± 0.75) had no significant difference with that of medium (5.00 sec^{-1} ± 0.64) (P>0.05). On R_2 mapping, the Free-SPIO signal intensity (75.61 sec^{-1} ± 0.20) was significant higher than that of B.*longum*-SPIO (2.70 sec^{-1} ± 0.11) (P<0.001), whereas the signal intensity of B.*longum* had no significant differences with that of medium (P<0.05).

By comparing the B.*longum*-SPIOs with the Free-SPIOs, we observed that with identical concentrations of iron in the phantom, B.*longum*-SPIOs showed higher R_2^* values compared with Free-SPIOs (Fig 4-c). On the other hand, R_2 measurements were higher for the Free-SPIOs than for the B.*longum*-SPIOs (Fig 4-d). Both the R_2 and the R_2^* had a linear relation to the number of tagged bacteria. However, the slope for the R_2^* effects was 31.25-fold higher (6.25×10^{-5} mL/bacteria.sec) than the slope for the R_2 effects (0.2×10^{-5} mL/bacteria.sec). Similarly, the R_2 and the R_2^* had a linear relation to the concentration of Free-SPIOs (Fig 5-a). Nevertheless, the slope for the R_2^* effects was only 1.99-fold higher (4.39×10^{-5} mL/μg.sec) than that for the R_2 effects (2.21×10^{-5} mL/μg.sec) (Fig 5-b).

In vivo MR imaging

The signal intensity was inhomogenous on R_2^* and R_2 mapping after injection the medium containing B.*longum*-SPIO and Free-SPIOs respectively into the subcutaneous HCC on the rats' back, and the signal intensity of B.*longum*-SPIO was prevalent higher than that of Free-SPIO. However, on R_2 mapping the B.longum-SPIO's signal intensity was lower than the Free-SPIOs' signal intensity. No matter on R_2^* mapping or on R_2 mapping, the signal intensity of bacteria (non-labeled with SPIO) was similar with that of medium.

Before injection of the medium containing B.*longum*-SPIO via the tail vein, on T_2WI and T_2^*WI, tumor signal intensity showed relatively homogeneous in six rats. However, 15 days after injection of B.*longum*-SPIO, the tumor signal intensity decreased slightly on T_2WI but significantly on T_2^*WI, and the hypo-intensity area was enlarged obviously in all our experimental animals. Iron staining particles is presented widespread in hypoxia and/or necrosis areas of tumor, and in some areas rod shaped iron staining particles was aggregated which morphologic changes is consistent with B.*longum*. On the other hand, 15 days after injection of Free-SPIO, on T_2^*WI, there was no obvious T_2^* shorted effect, and there was also no obvious iron-stained particle was detected within the experimental tumors.

Discussion

Labeling cells with SPIOs has been reported to be a sensitive and noninvasive method for tracking various cells such as monocytes [8, 9], bone marrow stem cells, embryonic stem cells [10, 11], mesenchymal stem cells [12] , T cells, macrophages, and Smooth Muscle Cells [13, 14] et al . Anaerobes such as C.*novyi*-NT and B.*longum* are much smaller than these cells, and have been shown to be potential nontoxic therapeutic agents in experimental tumors[15-20] or be armed with anti-cancer gene[5, 21-24] for malignant tumor treatment. To our knowledge, whether they could be labeled with SPIOs, then targeted tumor and detected by MRI within tumor hasn't been reported until now. Although bacteria had been visualized in real time using luciferase-catalyzed luminescence and green fluorescent protein fluorescence[7, 25], compared with MRI, these techniques were with lower spatial resolution and were performed with complexity. So we decided to label B.*longum* and C.*novyi*-NT, which were commonly used in present study, and to detect them in the tumor by MRI. Such technique might provide researchers with the ability to monitor these microorganisms and might even to quantitatively measure them with MRI.

The bacteria pellets precipitated at the bottom of tubes after centrifuge were different form each other among the four groups. After co-culturing B.*longum* with SPIOs, B.*longum*-SPIO's color was rust which demonstrated that SPIOs were swallowed by B.*longum* or were adhered to them, and the distribution of SPIOs was changed. There were no pellets at the bottom of tube containing Free-SPIO or Medium. Further electron micrography showed it was B.*longum* englobed SPIOs, and produced different diameter iron particles (50-100nm magnetosomes) within them. For C.*novyi*-NT, SPIOs were found not only within the whole body of bacteria but also within spore's cyst. We then presumed that SPIOs were embedded into spores during sporulation. The Prussian staining performed also provided evidences that B.*longum* and C.*novyi*-NT could be labeled by SPIOs. The colony number formed by B.*longum*-SPIO had no difference with that formed by B.*longum*, which illustrated that the bacteria activity hadn't been changed greatly. However, our method is not accurate in detecting the bacteria activity. Accurate systems should be performed in the future such as identifying different bacterial metabolin to further discuss the activity after they were tagged with SPIOs.

In vitro a linear relationship was observed between R_2 and R_2^* values and the number of B.*longum*-SPIO. We also observed a linear relationship between R_2 and R_2^* values and iron concentration in the phantom. For Free-SPIOs, R_2 and R_2^* showed similar relaxation rates. However, compared with Free-SPIOs, the bacteria-bound SPIOs revealed substantially higher R_2^* values and substantially lower R_2 values. The C.*novyi*-NT labeled with SPIO had similar MR imaging.

When SPIO particles are compartmentalized or phagocytized, and then many larger magnetosomes formed in bacteria, an inhomogeneous magnetic field is generated.

This may be addressed theoretically by applying the static dephasing regime theory. The change in relaxivity, depending on the compartmentalization status, reveals the difficulties in bacterium quantification because R_2 and R_2^* values depend not only on the iron concentration but also on the SPIO distribution.

The magnetic ferrite (Fe_3O_4) particles could be reconstructed as single magnetic domain at 50 nm, and then optimal ferromagnetism was obtained. Too larger or too smaller particles would destroy their ferromagnetism.

The SPIO particles are hepatic tissue specific MR contrast which will be uptaken by Kupffer cells in liver, shorten tissue T_2^*, and cause signal decreasing in corresponding area. However, the signal won't decrease in HCC when enhanced by SPIO because of deficiency of Kupffer cells which can be different from benign tumor. After percutaneous intra-tumor injection with B.*longum*-SPIO or SPIO, the signal intensity on R_2 and R_2^* reconstructed imaging was similar with that in vitro. However, the signal intensity was inhomogeneous because of the inhomogeneous diffusion after injection. So, the quantitation of signal intensity in vivo was difficult.

After 15 days, areas of tumors injected with B.*longum*-SPIO via tail vein still demonstrated hypointensity on T_2^*WI. Histological examination showed iron staining particles which might show as rod shape in the necrotic areas of tumor. We considered that this was because of the growth of B.*longum*-SPIO in the tumors. However, after injection with Free-SPIO for 15 days, T_2^* wasn't shorten in areas of the tumor on T_2^*WI. This might be contributed to that the SPIO particles had been metabolized or lacking Kupffer cells in the tumor which causing SPIO can't persistent exist intratumorally.

Conclusion

SPIO could be employed to label B.*longum* and C.*novyi*-NT. B.*longum*-SPIO and Free-SPIO has different MR imaging. The number of B.*longum*-SPIO has linear relationship with the R_2 and R_2^* value which might be used to quantitate B.*longum*. The C.*novyi*-NT has the similar phenomenon. T_2^* was shortened by B.*longum*-SPIO within tumor, and therefore MRI might be a noninvasive method to trace anaerobe such as B.*longum* and C.*novyi*-NT.

Acknowledgement

The authors are extending their sincerest gratitude to Dr. Ji Yang, Dr. Xingrong Yang, and Dr. Zhengdong Fang for their assistance in discussing this manuscript. The C.*novyi*-NT spores were kindly provided by professors Bert Vogelstein & Kenneth W. Kinzler at Johns Hopkins University in USA.

References

[1] Kimura NT, Taniguchi S, Aoki K, Baba T. Selective localization and growth of Bifidobacterium bifidum in mouse tumors following intravenous administration. Cancer Research 1980;40:2061-2068

[2] Cheong I, Huang X, Bettegowda C, et al. A bacterial protein enhances the release and efficacy of liposomal cancer drugs. Science 2006;314:1308-1311

[3] Zhao M, Yang M, Li XM, et al. Tumor-targeting bacterial therapy with amino acid auxotrophs of GFP-expressing Salmonella typhimurium. Proceedings of the National Academy of Sciences of the United States of America 2005;102:755-760

[4] Jain RK, Forbes NS. Can engineered bacteria help control cancer? Proc Natl Acad Sci U S A 2001;98:14748-14750

[5] Forbes NS. Profile of a bacterial tumor killer. Nature Biotechnology 2006;24:1484-1485

[6] Lemmon MJ, van Zijl P, Fox ME, et al. Anaerobic bacteria as a gene delivery system that is controlled by the tumor microenvironment. Gene Ther 1997;4:791-796

[7] Yu YA, Shabahang S, Timiryasova TM, et al. Visualization of tumors and metastases in live animals with bacteria and vaccinia virus encoding light-emitting proteins. Nature Biotechnology 2004;22:313-320

[8] Bulte JWM, Duncan ID, Frank JA. In vivo magnetic resonance tracking of magnetically labeled cells after transplantation. Journal of Cerebral Blood Flow and Metabolism 2002;22:899-907

[9] Zelivyanskaya ML, Nelson JA, Poluektova L, et al. Tracking superparamagnetic iron oxide labeled monocytes in brain by high-field magnetic resonance imaging. Journal of Neuroscience Research 2003;73:284-295

[10] Jendelova P, Herynek V, Urdzikova L, et al. Magnetic resonance tracking of transplanted bone marrow and embryonic stem cells labeled by iron oxide nanoparticles in rat brain and spinal cord. In: *Satellite Symposium on Neural Stem Cells and Brain Repair*. Prague, CZECH REPUBLIC, **2003**:232-243

[11] Hinds KA, Hill JM, Shapiro EM, et al. Highly efficient endosomal labeling of progenitor and stem cells with large magnetic particles allows magnetic resonance imaging of single cells. Blood 2003;102:867-872

[12] Bos C, Delmas Y, Desmouliere A, et al. In vivo MR imaging of intravascularly injected magnetically labeled mesenchymal stem cells in rat kidney and liver. Radiology 2004;233:781-789

[13] Kraitchman DL, Heldman AW, Atalar E, et al. In vivo magnetic resonance imaging of mesenchymal stem cells in myocardial infarction. Circulation 2003;107:2290-2293

[14] Riviere C, Boudghene FP, Gazeau F, et al. Iron Oxide Nanoparticle-labeled Rat Smooth Muscle Cells: Cardiac MR Imaging for Cell Graft Monitoring and Quantitation. In: *Radiology*, **2005**:959-967

[15] Dang LH, Bettegowda C, Huso DL, Kinzler KW, Vogelstein B. Combination bacteriolytic therapy for the treatment of experimental tumors. Proc Natl Acad Sci U S A 2001;98:15155-15160

[16] Wei MQ, Mengesha A, Good D, Anne J. Bacterial targeted tumour therapy-dawn of a new era.

Cancer Letters 2008;259:16-27
[17] Hawkins LK, Lemoine NR, Kirn D. Oncolytic biotherapy: a novel therapeutic plafform. Lancet Oncol 2002;3:17-26
[18] Minton NP. Clostridia in cancer therapy. Nature Reviews Microbiology 2003;1:237-242
[19] Bettegowda C, Dang LH, Abrams R, et al. Overcoming the hypoxic barrier to radiation therapy with anaerobic bacteria. Proceedings of the National Academy of Sciences of the United States of America 2003;100:15083-15088
[20] Diaz LA, Cheong I, Foss CA, et al. Pharmacologic and toxicologic evaluation of C-novyi-NT spores. Toxicological Sciences 2005;88:562-575
[21] Pawelek JM, Low KB, Bermudes D. Bacteria as tumour-targeting vectors. Lancet Oncology 2003;4:548-556
[22] Li X, Fu G-F, Fan Y-R, et al. Bifidobacterium adolescentis as a delivery system of endostatin for cancer gene therapy: selective inhibitor of angiogenesis and hypoxic tumor growth. Cancer Gene Ther 2003;10:105-111
[23] Yazawa K, Fujimori M, Amano J, Kano Y, Taniguchi S. Bifidobacterium longum as a delivery system for cancer gene therapy: Selective localization and growth in hypoxic tumors. Cancer Gene Therapy 2000;7:269-274
[24] Yazawa K, Fujimori M, Nakamura T, et al. Bifidobacterium longum as a delivery system for gene therapy of chemically induced rat mammary tumors. Breast Cancer Res Treat 2001;66:165-170
[25] Min J-J, Nguyen VH, Kim H-J, Hong Y, Choy HE. Quantitative bioluminescence imaging of tumor-targeting bacteria in living animals. Nat Protocols 2008;3:629-636

Fig-1 After shaking culture anerobically for 72 hr, four groups of tubes filled respectively with Medium alone, Free-SPIO, B.*longum*-SPIO and B.*longum* were centrifuged and demonstrated different appearance. The B.*longum*-SPIO pellets showed rust, even and opaque, while the color of its medium becomes light when compared with that of Free-SPIO. The B.*longum* pellets showed ivory white, even and opaque, and the color of its medium was similar with that of B.*longum*-SPIO's medium. There was no any sediment in the culture tubes of G (Free-SPIO) and G (Medium). The C.*novyi*-NT test had the same phenomenon.

Fig-2 Transmission electron microscopy showed unlabeled B.*longum* (2a) and labeled B.*longum* (2b) with SPIO. The B.*longum*-SPIO contains a characteristic electron-dense sphere, ellipse or irregular-shaped crystal (about 50-100 nm) which mainly deposited along the midline of the bacteria cells. SPIO particles weren't also observed within C.*novyi*-NT spore unlabeled with SPIO (2c) and were appeared within C.*novyi*-NT spore tagged with SPIO (2d).

Fig-3 Prussian blue stain. (a)The whole bodies of some B.*longum*-SPIO cells were completely stained iron blue, and some cells stained with dark rust. (b) The B.*longum* cells (unlabeled with SPIO) were stained nuclear fast red (counterstain's color). (c) The C.*novyi*-NT-SPIO cells were also stained iron blue after shaking culture for 72hr. (d) The C.*novyi*-NT cells demonstrated also no iron blue but stained with nuclear fast red.

Fig-4 In vitro MR imaging of bacteria phantom. (a) With identical concentrations of iron in the phantom, on R_2^* mapping, B.*longum*-SPIO showed significant higher signal than that of Free-SPIO. (b) However, on R_2 mapping, the signal was higher for the Free-SPIO than for the B.*longum*-SPIO. No matter on R_2^* mapping or on R_2 mapping, the signal of B.*longum* has no differences with that of the medium. (c) With identical concentrations of iron in the phantom, B.*longum*-SPIOs showed higher R_2^* values compared with Free-SPIOs. (d) On the other hand, R_2 measurements were higher for the Free-SPIOs than for the B.*longum*-SPIOs.

Fig-5 (a) Both the R_2 and the R_2^* had a linear relation to the number of B.*longum*-SPIOs in the medium. The R_2^* value augmented rapidly with the increase of the number of B.*longum*-SPIOs, while the R_2 value had rarely changes when the number of B.*longum*-SPIOs increased. (b) The R_2 and the R_2^* had a linear relation to the concentration of SPIO. Nevertheless, the R_2^* effects was slightly higher than the R_2 effects.

Fig-6 The different ROI appearances on R_2^* and on R_2 mapping of subcutaneous McA-RH7777 hepatocellular carcinoma after intro-tumor injection of Free-SPIOs (ROI 1) and B.*longum*-SPIO (ROI 2).

Fig-7 Buffalo rats with hepatocellular carcinoma treated by injection of the medium containing B.*longum*-SPIO via the tail vein and detected by T2WI and T_2^*WI.(a) T2WI before injection.(b) T_2^*WI before injection. (c) T2WI after injection. (d) T_2^*WI after injection. (e) Prussian bule staining showed iron staining particles scattered in the tumor necrotic area (×1000). (f) Aggregated rod shape Prussian-blue-stained bacteria are distributed within the tumor (×1000).

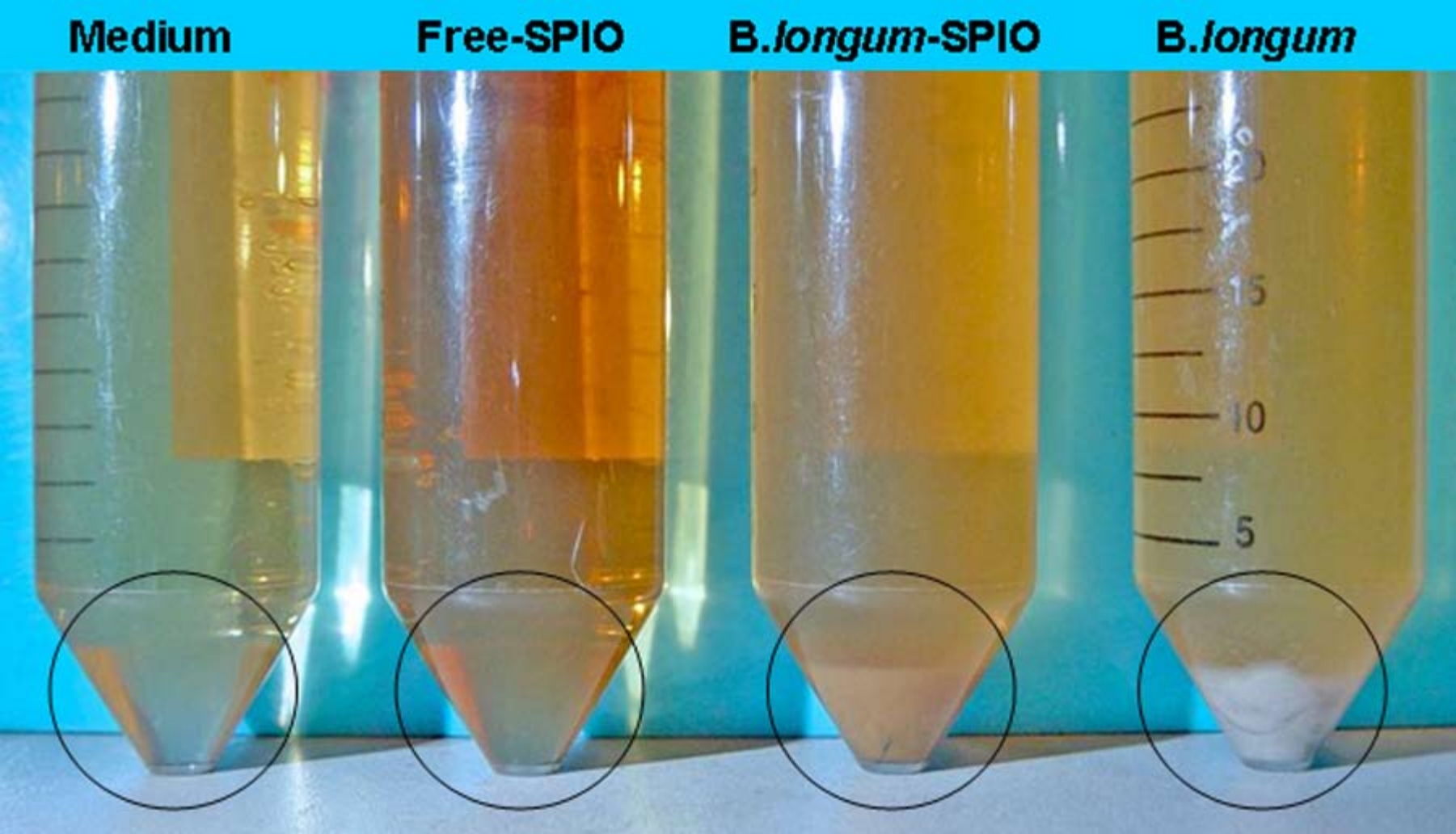
Medium
Free-SPIO
B.longum-SPIO
B.longum
15
10
5

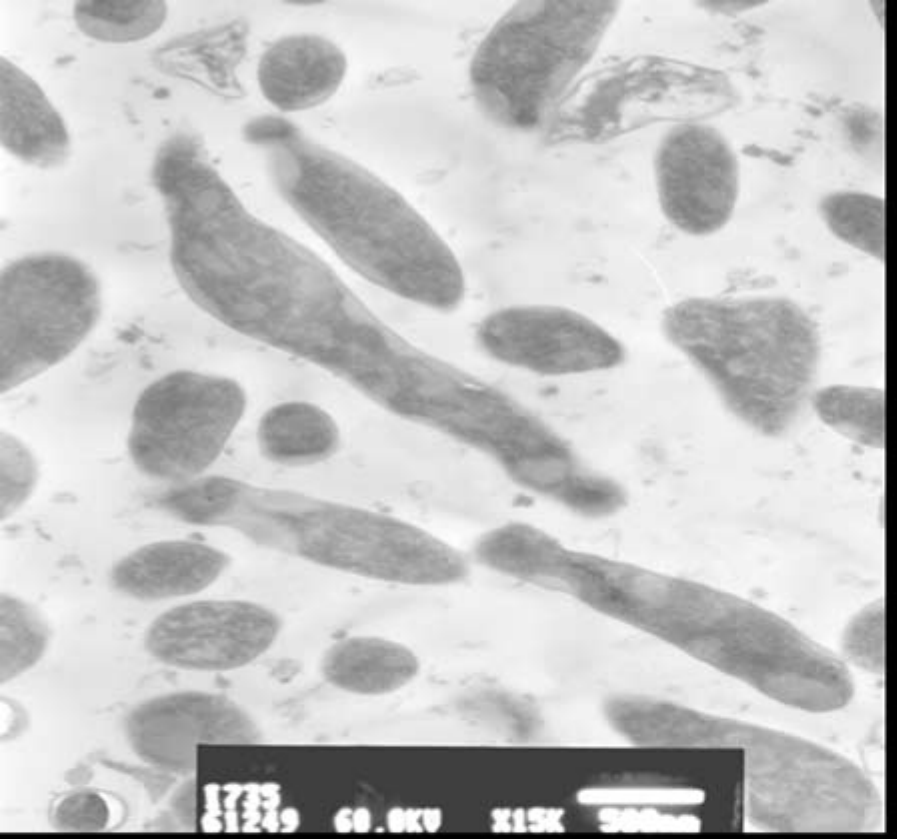
60.0KV X15K

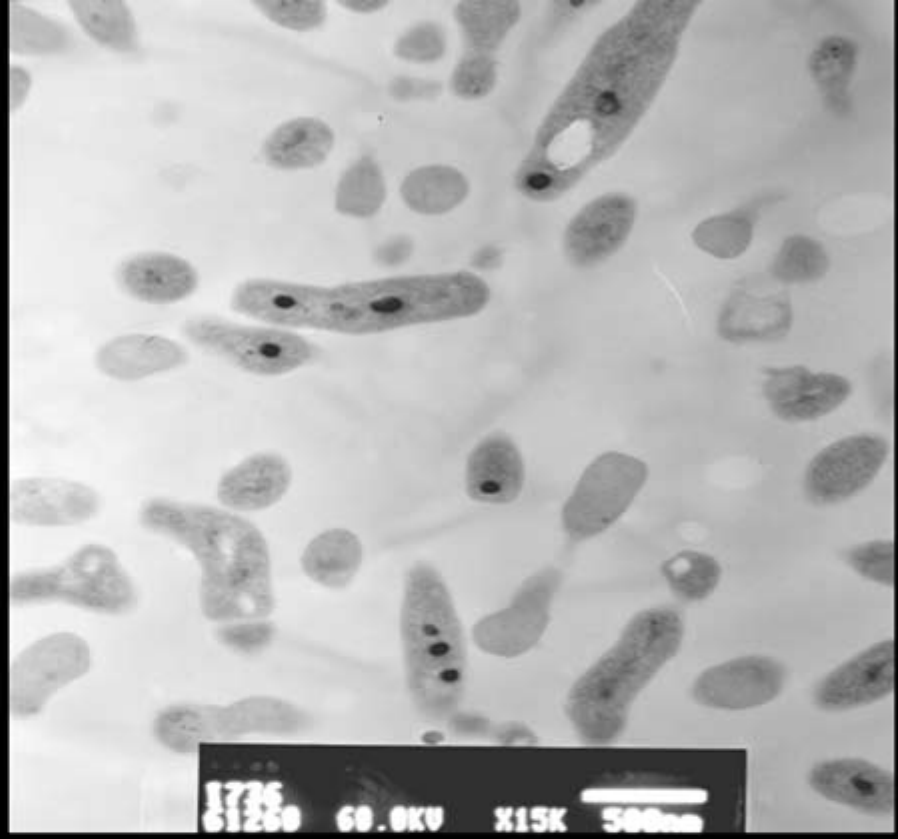
60.0KV X15K

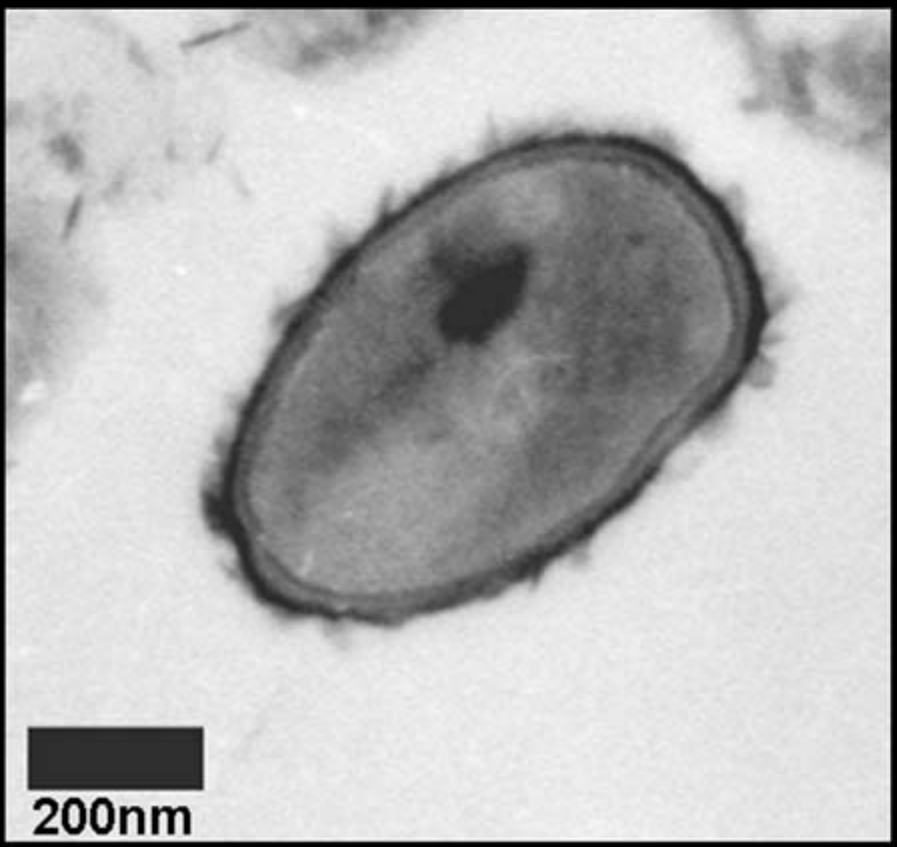
200nm

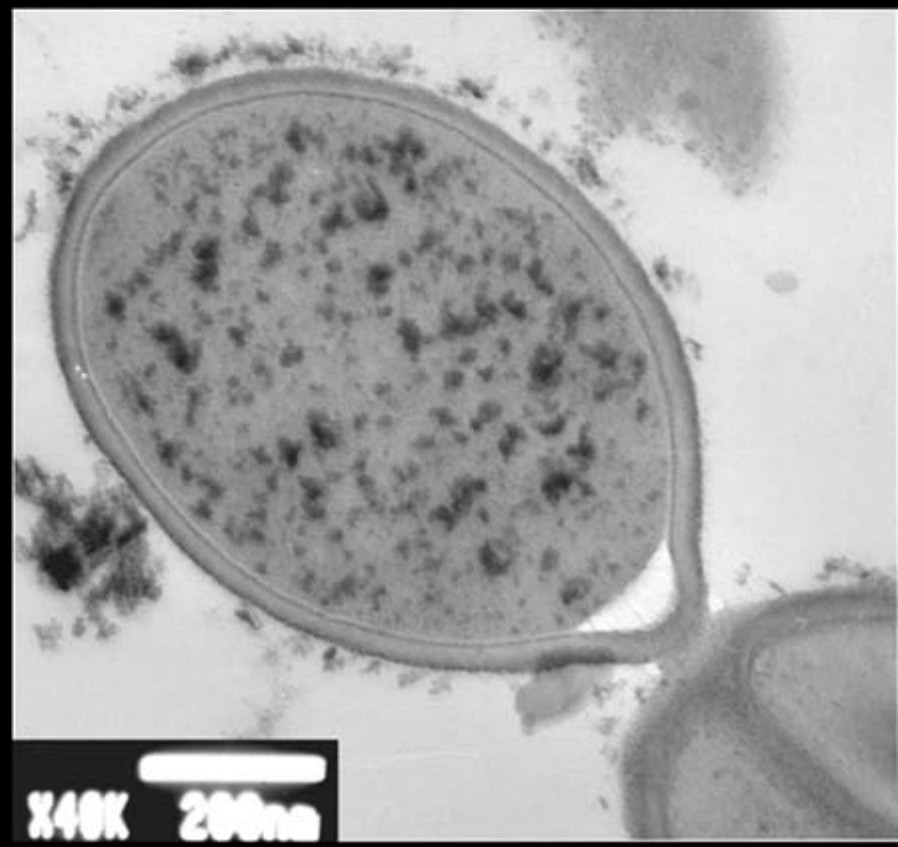
X40K

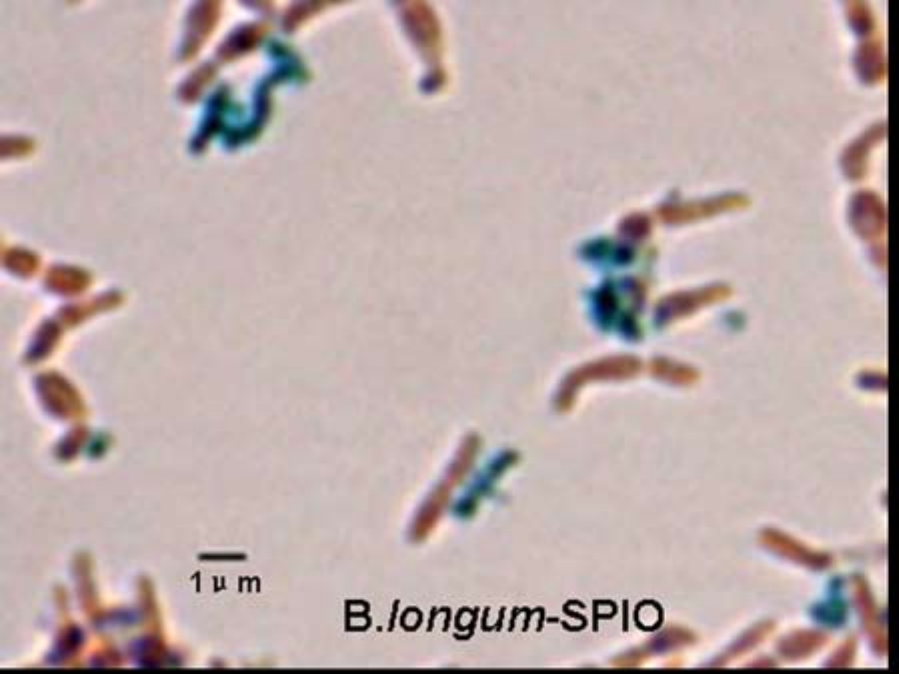
1 µ m
B.*longum*-SPIO

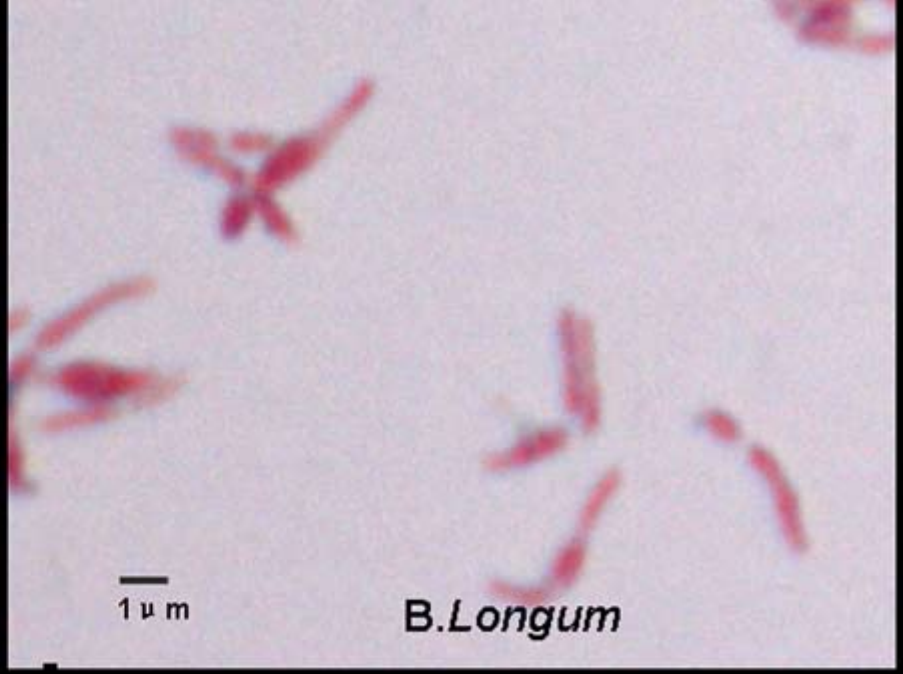
1 µ m
B.*Longum*

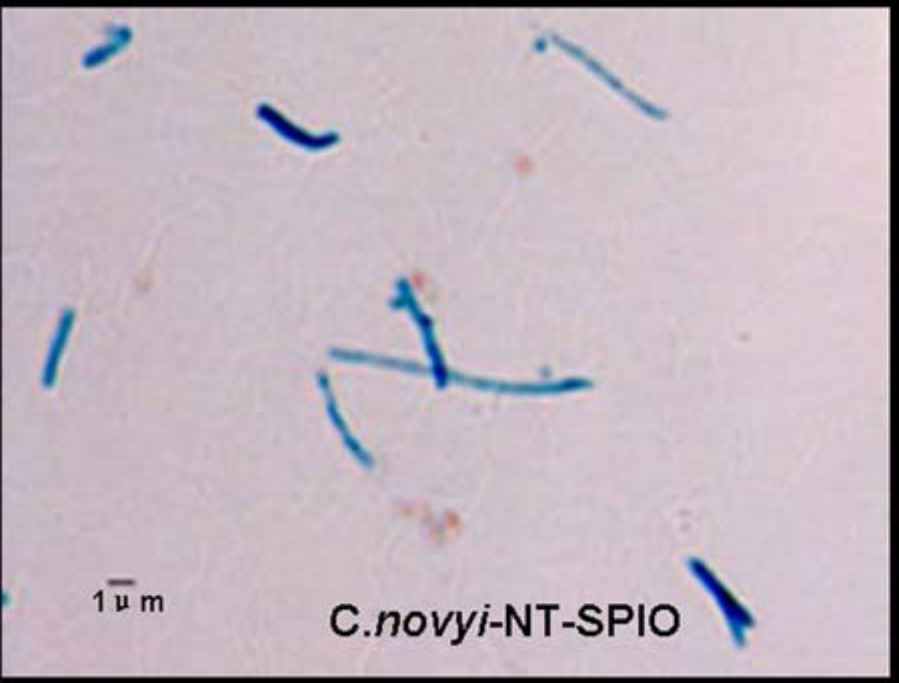
1 µ m
C.*novyi*-NT-SPIO

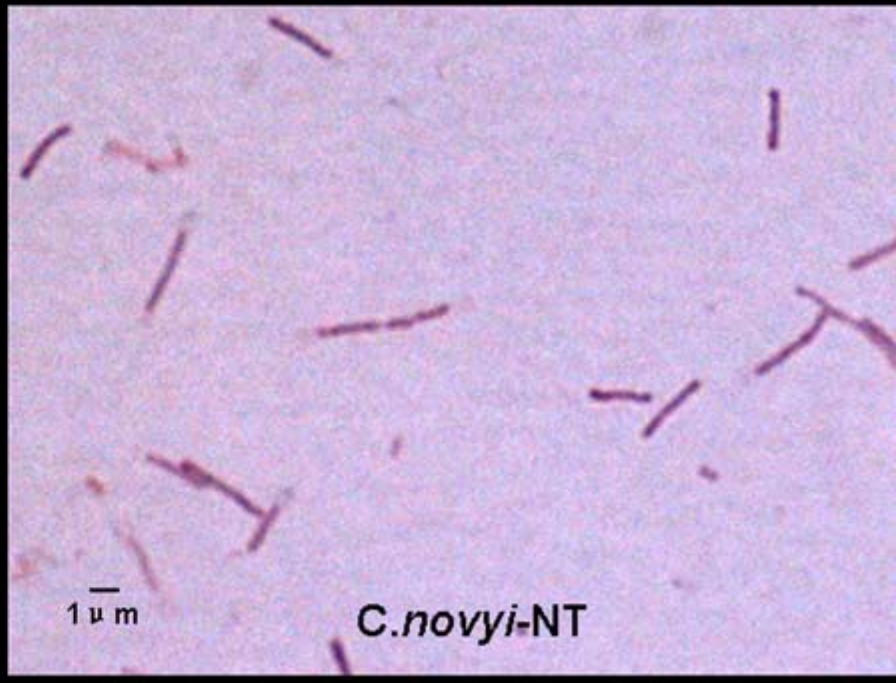
1 µ m
C.*novyi*-NT

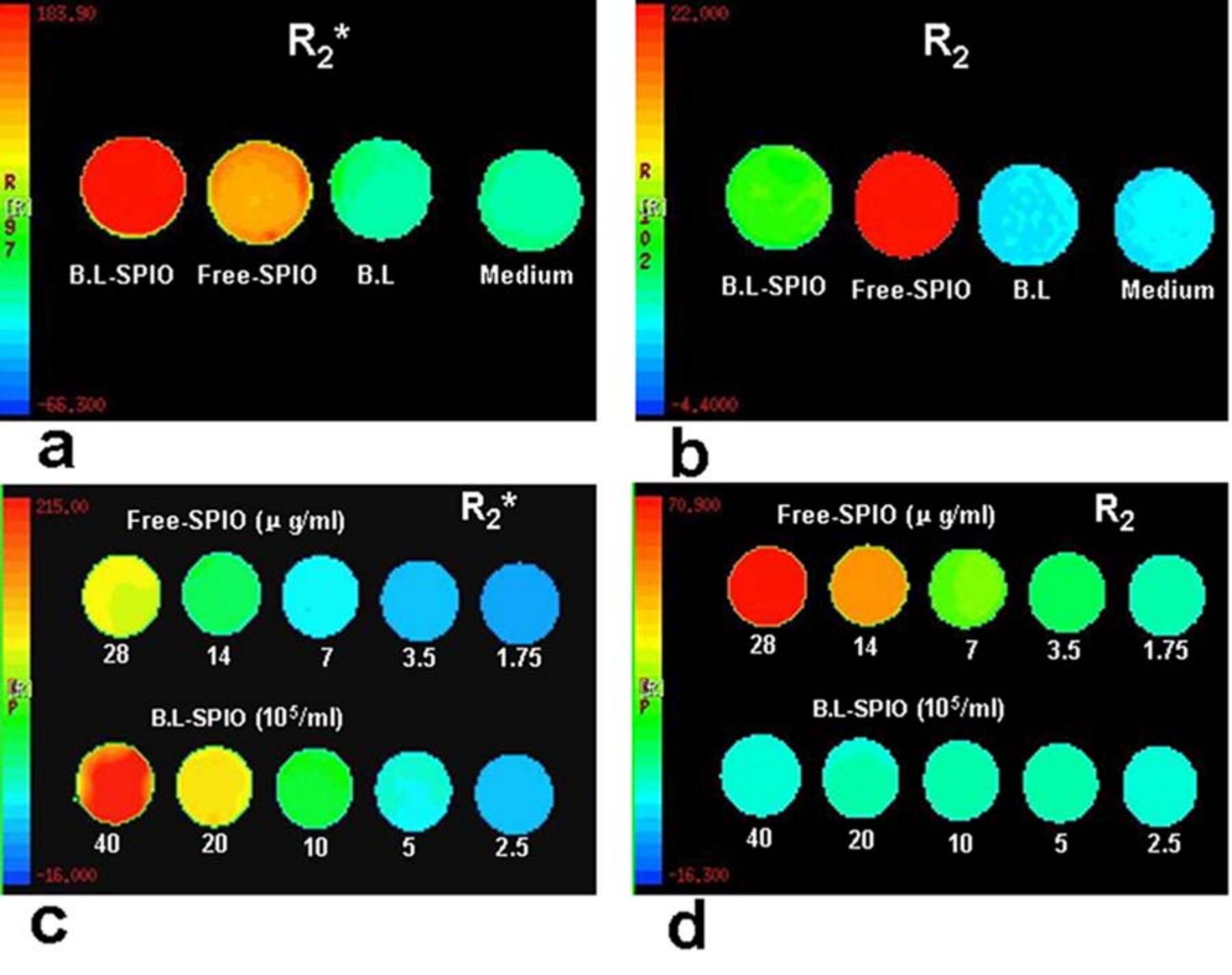
183.90
R2*
B.L-SPIO
Free-SPIO
B.L
Medium
-66.300
a
22.000
R2
B.L-SPIO
Free-SPIO
B.L
Medium
-4.4000
b
215.00
Free-SPIO (μ g/ml)
R2*
28
14
7
3.5
1.75
B.L-SPIO (10⁵/ml)
40
20
10
5
2.5
-16.000
c
70.900
Free-SPIO (μ g/ml)
R2
28
14
7
3.5
1.75
B.L-SPIO (10⁵/ml)
40
20
10
5
2.5
-16.300
d

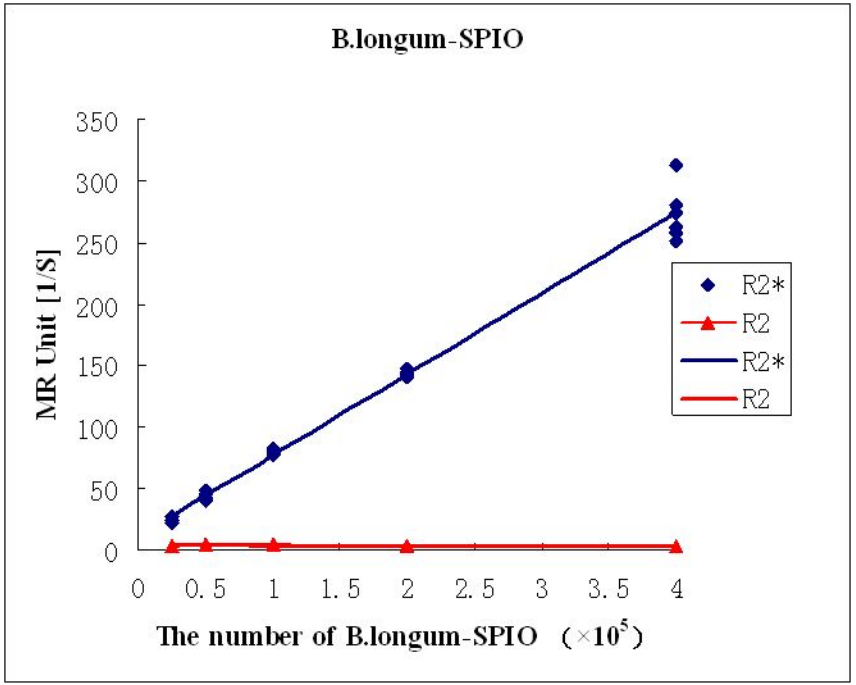
B.longum-SPIO
MR Unit [1/S]
350
300
250
200
150
100
50
0
0
0.5
1
1.5
2
2.5
3
3.5
4
The number of B.longum-SPIO (×10^5)
R2*
R2
R2*
R2

a

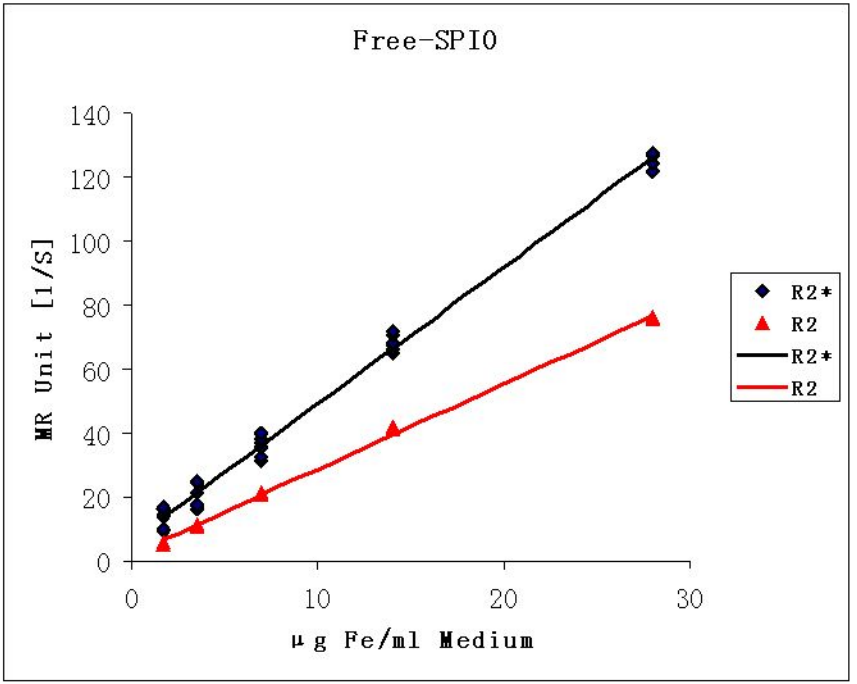
Free-SPIO
MR Unit [1/S]
140
120
100
80
60
40
20
0
0
10
20
30
μg Fe/ml Medium
R2*
R2
R2*
R2

b

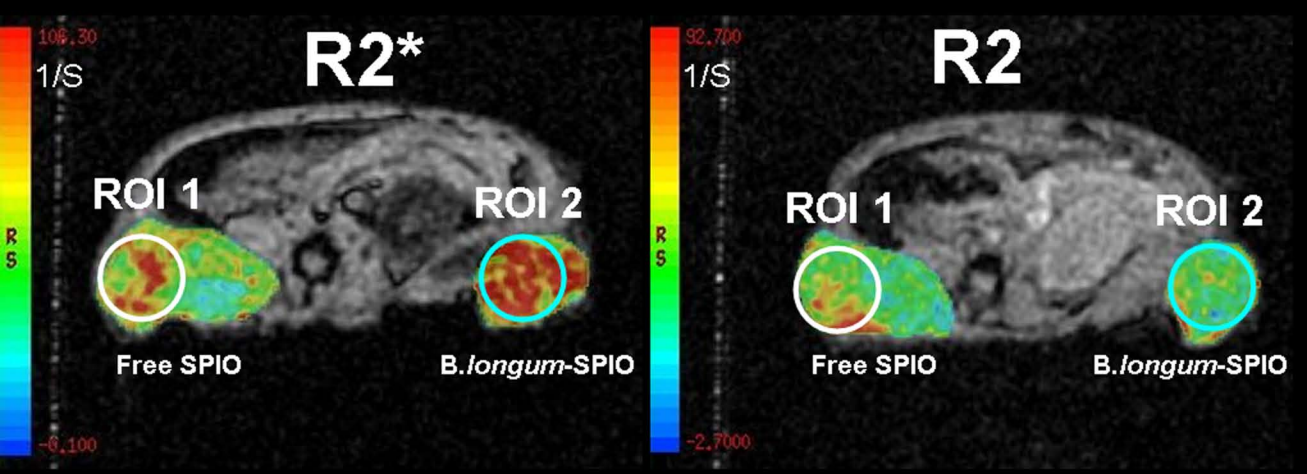
R2*
1/S
ROI 1
ROI 2
Free SPIO
B.longum-SPIO
R2
1/S
ROI 1
ROI 2
Free SPIO
B.longum-SPIO

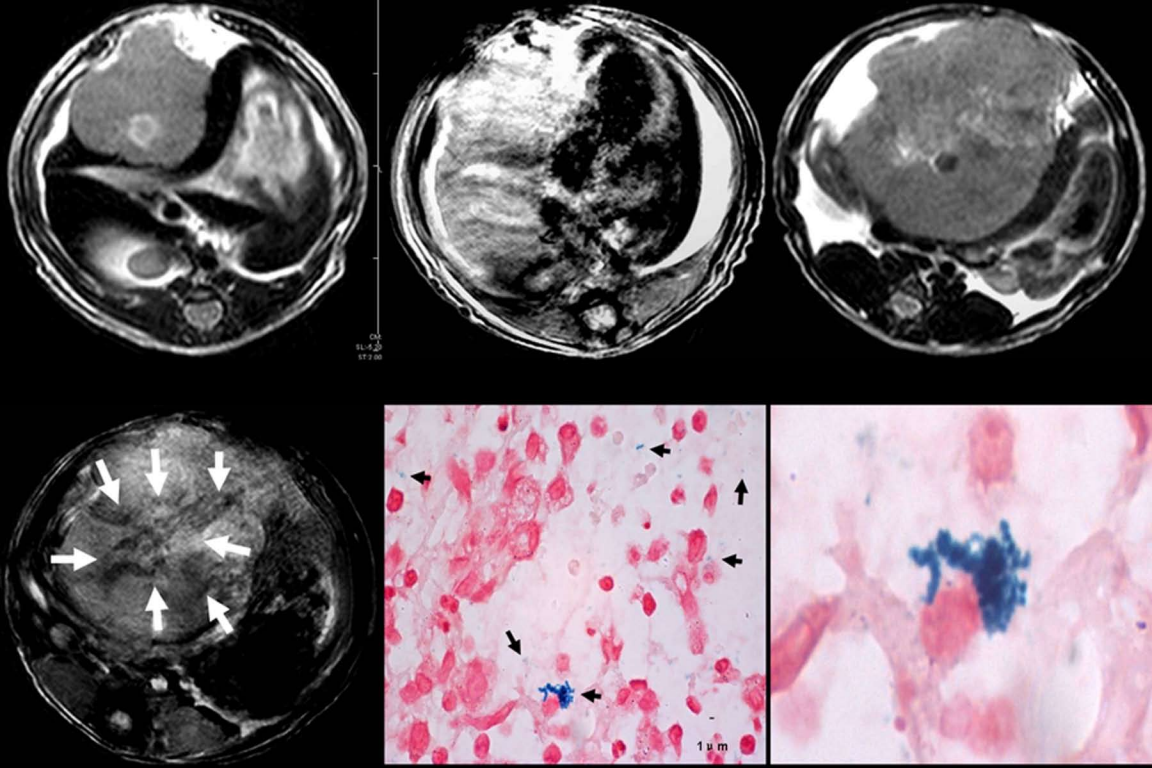
1 µ m